ELSEVIER

Journal of Nuclear Materials 280 (2000) 331–344

journal of nuclear materials

www.elsevier.nl/locate/jnucmat

Synthesis of atom probe experiments on irradiation-induced solute segregation in French ferritic pressure vessel steels

P. Auger [a], P. Pareige [a,*], S. Welzel [a], J-C. Van Duysen [b]

[a] *Groupe de Physique des Matériaux, UMR CNRS 6634, Université-INSA de Rouen, 76821 Mont Saint Aignan, France*
[b] *EDF, Centre de Recherche des Renardières, 77250 Moret sur Loing, France*

Received 7 December 1999; accepted 30 March 2000

Abstract

Microstructural changes due to neutron irradiation cause an evolution of the mechanical properties of reactor pressure vessels (RPV) steels. This paper aims at identifying and characterising the microstructural changes which have been found to be responsible in part for the observed embrittlement. This intensive work relies principally on an atom probe (AP) study of a low Cu-level French RPV steel (Chooz A). This material has been irradiated in in-service conditions for 0–16 years in the frame of the surveillance program. Under this aging condition, solute clustering occurs (Cu, Ni, Mn, Si, P, ...). In order to identify the role of copper, experiments were also carried out on Fe–Cu model alloys submitted to different types of irradiations (neutron, electron, ion). Cu-cluster nucleation appears to be directly related to the presence of displacement cascades during neutron (ion) irradiation. The operating basic physical process is not clearly identified yet. A recovery of the mechanical properties of the irradiated material can be achieved by annealing treatments (20 h at 450°C in the case of the RPV steel under study, following microhardness measurements). It has been shown that the corresponding microstructural evolution was a rapid dissolution of the high number density of irradiation-induced solute clusters and the precipitation of a very low number density of Cu-rich particles.

PACS: 61.16.Fk; 61.80.Hg; 28.41.Qb; 61.82.Bg

1. Introduction

Ferritic steels of reactor pressure vessels (RPV) are subjected to irradiation with high energy neutrons ($E > 1$ MeV) from the reactor core, arising from nuclear reactions. The irradiation disrupts the crystalline lattice and atoms are displaced, creating several possible types of irradiation-induced damage: vacant lattice sites and atoms occupying interstitial positions (Frenkel pairs), vacancy and/or interstitial clusters, microvoids, dislocation loops, solute clusters or precipitates, ... These changes in the microstructure and microchemistry cause an evolution of the mechanical properties of the material. More precisely, the metal hardens and embrittlement may occur as indicated by the shift, towards higher temperatures, of the ductile-to-brittle transition temperature. This makes the RPV, in the region of the beltline, more susceptible to brittle fracture during pressurised thermal shock transients. This may result in a premature shutdown of the plant if the degree of embrittlement becomes severe.

To maintain a strict control over the RPV steels it is a necessity to have an accurate description of the changes that occur in the microstructure. The progress in the understanding of microstructural evolution and related physical mechanisms has been mainly the consequence of the improvement of advanced characterisation tools such as small angle neutron scattering (SANS), transmission electron microscopy (TEM) including high resolution electron microscopy (HREM), TEM with

* Corresponding author. Tel.: +33-2 35 14 68 78; fax: +33-2 35 14 66 52.
E-mail address: philippe.pareige@univ-rouen.fr (P. Pareige).

0022-3115/00/$ - see front matter
PII: S0022-3115(00)00056-8

field emission gun (FEGSTEM), positron annihilation (PA) and also field ion microscopy (FIM) and atom probe techniques (AP and 3D AP).

In addition to the need to maintain adequate safety margins for vessel operation, the economic incentives for extending the lifetime of current RPVs have motivated research (mainly in Russia and US) on methods of mitigating embrittlement. Thermal annealing treatments have been identified as a suitable means to recover the mechanical properties. Recent studies of this thermal recovery, [1–3] including in situ RPV anneals have provided an extensive set of data describing the mechanical properties.

Although the mechanical behaviour of these materials is relatively well known, limited information is available on irradiation-induced microstructural changes.

This study relies principally on the use of AP and 3D AP instruments which are particularly well suited to characterise nanostructural features [4,5]. In this paper, detailed descriptions of the nano-transformed phases developed during neutron irradiation are presented. A precise description of each of the basic mechanisms (voids, point defects, interstitial loops, etc.) needs the combination of data from complementary techniques. However, in order to isolate each consequence of a specific kind of defects (displacement cascades or Frenkel pairs) experiments were performed on electron as well as ion irradiated materials. As it has been previously shown [6,7], copper plays an important role in the embrittlement of RPV steels. This is the reason why experiments were also performed on binary Fe–Cu model alloys. The materials studied were obtained from the Electricité de France Research Centre in the framework of the French surveillance program.

This paper is divided in four major parts. After a brief introduction to the AP techniques in Section 2, effects of neutron irradiation in the French RPV steels are presented in Section 3. Section 4 is dedicated to the study of model alloys irradiated in various conditions: neutrons, ions and electrons. In Section 5, results on the effect of thermal annealing of French neutron irradiated RPV steels are presented and discussed.

2. AP techniques

Among the various microanalytical techniques which are used in material science, the AP invented by Müller and co-workers [8], 30 years ago, is the instrument which provides the highest spatial resolution. The lateral resolution at the specimen surface is a few nanometers while depth resolution is a single atomic layer. Another advantage of AP techniques is their quantitativity. Under proper experimental conditions [9], concentrations are reliable and directly proportional to the number of ions of each species collected from the specimen. The principle is based on the field evaporation of surface atoms and their mass identification by time-of-flight mass spectrometry [9]. The mass resolution is close to $M/\Delta M = 300$ at half maximum. The high electric field required for the field evaporation process (30–50 V/nm) is achieved by applying a high voltage (2–20 kV) to the sample prepared in the form of a sharp pointed needle [9].

Implementation of electrostatic lens or mirrors, usually named 'energy compensated' systems, on conventional AP (Energy Compensated Atom Probe, ECAP) highly improves the resolution of the mass spectrum. An electrostatic lens of 'Poschenrieder' type equips one of the APs of our laboratory [4]. The high mass resolution ($M/\Delta M = 2000$) is necessary to identify unambiguously all chemical species, particularly Ni, Mo and Cu which are detected with mass difference of 1/6 of an atomic mass unit (a.m.u.). The result of such an ECAP analysis is a linear concentration profile established for each species. The lateral resolution is chosen (from 0.5 to 3 nm) and kept constant while the depth resolution is strictly one atomic layer.

Improvement of the AP technique was realised with the implementation of a position-sensitive detector on the instrument. This multidetection system has a great advantage to give in addition to their identification, the position of the detected ions even for simultaneous impacts and multiple time-of-flight events [10]. Thus, quantitative composition data, as well as reliable positions are obtained. This new instrument named, in France, Tomographic Atom Probe (TAP) is schematically depicted in Fig. 1.

Ion impacts on the detector are localised with a precision close to 0.1 mm. This corresponds to an accuracy of atom positioning at the tip surface better than 0.1 nm. The actual spatial resolution is however degraded from this value due to aberrations of ion trajectories in the close vicinity of the tip surface. The maximum resolution is between 0.3 and 0.5 nm. By field evaporation of surface atoms, the material is explored in depth, layer after layer. For each evaporated layer, the related 2D element cartography is calculated and a 3D reconstruction of the probed volume ($\sim 10 \times 10 \times 100$ nm^3) can finally be achieved by combining successive 2D maps. Reconstructed analysed volumes are typically composed of a few 10^5 atoms. The data set is subsequently treated with a graphic work station using advanced 3D image computer software.

3. Neutron irradiation of a French RPV steel

3.1. Material description

The experiments were performed on a steel irradiated in the Chooz A surveillance program (France). This

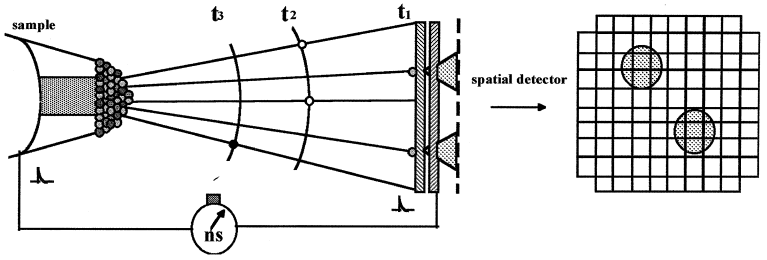

Fig. 1. Schematic representation of the TAP. (left) The conventional system depicting field ion evaporation and the time-of-flight measurements. (right) A presentation of the multi-anode position-sensitive detector.

Table 1
Chemical compositions (wt% and at.%; iron is balance) of the Chooz A pressure vessel steel

Elements	C	S	P	Si	Cr	Mo	Mn	Ni	V	Al	Co	Cu
wt%	0.16	0.005	0.012	0.32	0.16	0.39	1.26	0.57	0.02	0.024	0.020	0.090
at.%	0.74	0.009	0.021	0.63	0.17	0.22	1.26	0.53	0.02	0.049	0.018	0.078

program has been carried out since 1970 with 8 capsules containing Charpy V-notch test specimens machined in materials representative of the pressure vessel core zone. A description of the Chooz A surveillance program is given in Ref. [11]. All the samples used for this microstructural study were taken from these Charpy test specimens.

3.1.1. Chemical composition

The studied steel was austenitized at 910°C for 1 h, water quenched, then tempered at 660–670°C for 4 h and finally stress relieved at 600°C for 28 h. The material is of 16MND5 type with a ferritic–bainitic structure which contains carbides and a high density of dislocations partially organised in sub-boundaries. Some regions are fully bainitic whereas some others contain about 60% of bainite and 40% of ferrite. The chemical composition of this steel is given in Table 1. It must be noted that the concentration of the 'well-known' highly embrittling elements (Cu, P) is rather low.

3.1.2. Irradiation conditions

Chooz A, now out of service, was the oldest PWR in service in France. The operating conditions of this reactor are fully described in Ref. [12]. The surveillance capsules have been suspended under the lower core plate. This location results in a very high flux gradient along the length of the Charpy V specimens. For each capsule, the fluxes were measured with 10 copper activated dosimeters set on three levels. It is considered that the temperature of all these Charpy specimens was equal to that of the inlet water: 270°C.

Capsules, irradiated by energetic neutrons ($E > 1$ MeV) from the core, were withdrawn from the reactor after about 2–16 years of service. On an average, neutron fluxes were of the order of $1–2 \times 10^{11}$ n cm^{-2} s^{-1}, thus the received fluences range from 0.5 to 17×10^{19} n cm^{-2}, that is to say from 1 to 20×10^{-2} NRT dpa [13].

3.1.3. Evolution of mechanical properties

This steel hardens with increasing fluences. A concomitant increase of temperature of the ductile-to-brittle transition (ΔRT_{NDT}) is observed (Table 2).

3.1.4. Experimental

In order to ascertain the specific role of neutron irradiation, irradiated samples were compared to unirradiated materials (reference material). The experimental procedures required for reliable data to be obtained are fully described elsewhere [14–17].

Both ECAP and TAP were used:

- The ECAP, because of its high mass resolution ($M/\Delta M \sim 2000$) enables peak overlap to be avoided. Conversely, because of the monodimensional nature of these analyses, unavoidable spatial convolutions occur between the iron matrix and the tiny solute clusters which are formed during irradiation. The analysis of a pure solute particle may therefore lead to lower apparent levels.

Table 2
Amplitude of the shift of the ductile-to-brittle transition temperature (ΔRT_{NDT})

Fluence ($E > 1$ MeV, 10^{23} n m^{-2})	1.7	3.5	4.6	10
ΔRT_{NDT} (°C)	65	91	103	145

- This is one of the greatest advantages of the TAP to eliminate these spatial convolutions and to give access directly to the size, the morphology, the nature of the interface and the composition of each nanostructural individual event. The mass resolution of the TAP ($M/\Delta M \sim 200$) is however lower as compared to that of ECAP. Another advantage of TAP is both its higher spatial resolution and its larger analysis area (10 nm^2). Moreover, the larger analysed volume (some 10 times larger than with conventional AP) allows to increase the precision of number density measurement.

3.2. Irradiation-induced solute segregation in Chooz A steel

3.2.1. Experimental evidence of solute cluster formation during neutron irradiation

In order to achieve precise composition measurements in this multi-element material, random AP analyses (for ferrite) and selected area analyses (for carbides) were carried out with the ECAP. Random AP analysis involves the acquisition of a set of data (sequence of atoms) representing the collection and chemical analysis of the material along a thin cylinder, the diameter of which (1.5 nm in the case of our study) is the lateral resolution and the length may reach some hundred nanometers. Several random analyses of the same specimen are generally carried out in order to improve the statistical confidence in the measured composition. Conversely, for a selected area analysis, the surface of the specimen is first imaged and observed (FIM) and then the area of interest (small carbides for instance) is selected for analysis.

This experimental protocol was applied to several specimens of the Chooz A steel previously exposed to different neutron fluences ranging from 0.5 to 16×10^{23} n m^{-2} as well as to the reference specimen (unirradiated).

In order to characterise the microstructure of these materials (unirradiated and irradiated), analyses were performed on both the carbides and the matrix.

All of these specimens contain a high proportion of carbides because of their ferritic–bainitic structure. The more common features encountered are molybdenum-containing carbides and M_3C cementite carbides (with M = Fe, Mn, and to a lesser extent Cr or Mo). Table 3 shows the results of two representative analyses: one of a Mo_2C, the other of a M_3C carbides. These analyses were performed in the reference material. The uncertainties on concentration measurements are given with two statistical standard deviations ($\Delta X = 2\sigma_c$; with $\sigma_c = \sqrt{X(1-X)/N}$, where N is the number of atoms and X is the atomic concentration of one chosen chemical element).

These results concerning carbides are similar to those observed in previous analyses of US weld, forging and plate metals [18,19]. No change in composition and size of carbides can be attributed to the irradiation process. In addition, the AP results were compared to thermodynamic predictions [20]. The experimental compositions of cementite carbides are also in good agreement with the Thermocalc™ predictions for materials thermally aged at 600°C (temperature of the last stress relieve thermal treatment of the steel). This agreement indicates that irradiation has no significant impact on the evolution of the microchemistry of cementite carbides.

In contrast, differences between unirradiated and irradiated specimens appear in the ferrite phase. Fig. 2 represents series of concentration (atomic fraction) histograms related to the unirradiated (reference steel) and irradiated specimens (12×10^{23} n m^{-2}; ~180 NRT mdpa).

Such concentration histograms were derived from AP data as follows: collected ions were gathered into successive blocks ($N = 100$ atoms per block). Concentrations were calculated for each species in each block. The frequency of occurrence of a given concentration is represented, in Fig. 2, by a bar, the height of which is in the interval 0–1.

In the case where chemical elements are randomly distributed, the bar-chart must be similar to a binomial distribution, while if solute segregation occurs, a bimodal distribution arises. Statistical tests (χ^2) were used to compare binomial and experimental distributions. This permits the determination, under a chosen degree of confidence, as to whether the solute distribution is random or not.

Table 3
AP determination of the chemical compositions of Mo_2C and M_3C carbides encountered in the reference Chooz A steel

	C	Si	Fe	Cr	Mo	Mn	Ni
Mo_2C type							
X (at.%)	30.8	–	2.7	3.2	61.0	1.8	0.4
ΔX (at.%)	2.5	–	0.9	0.9	2.6	0.7	0.3
M_3C type							
X (at.%)	22.82	0.07	62.78	1.76	1.30	10.60	0.67
ΔX (at.%)	0.80	0.05	0.93	0.25	0.21	0.60	0.15

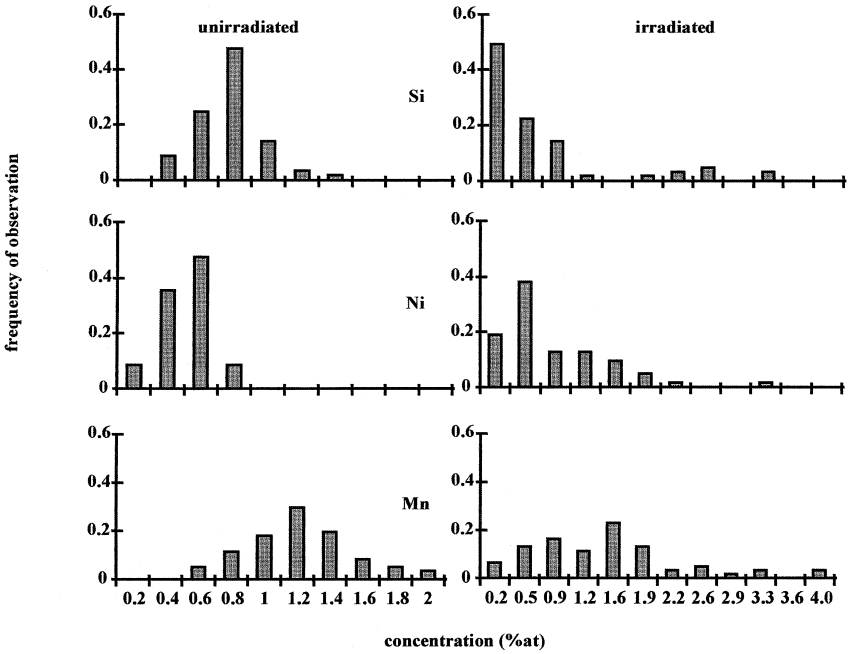

Fig. 2. Histograms depicting the observed frequencies of solute concentrations (ECAP data) versus the solute concentrations (Si, Ni, Mn); for unirradiated and irradiated materials (Chooz A steel, 12×10^{19} n cm^{-2}).

Fig. 2 clearly exhibits binomial-like distributions of solutes (Si, Ni, Mn) for the unirradiated specimen. A bimodal distribution is observed for the irradiated one. This is confirmed by χ^2 tests. These indicate that these elements are randomly dispersed in the ferrite solid solution in the reference steel and are prone to segregation under neutron irradiation.

In order to explore this phenomenon in more depth, concentration profiles of all the elements were generated. Fig. 3 refers to the same irradiated specimen and proves that the solutes Si, Ni, Mn, Cu, but also sometimes P, C, Mo, Cr, segregate to develop rather spherical clusters, the sizes of which range from 2 to 6 nm with an average around 3 nm.

For this highly irradiated specimen, the solute clusters were found with a high number density (of the order of 10^{24} m^{-3}). Sixteen of these clusters were analysed [14]. The main solute components are Si, Ni, Mn and Cu which represent about 15 at.% of the cluster. The concentration of these solutes shows a large variability from one cluster to another and is intrinsically weak as can be seen in Table 4. Local measurements performed with the TAP demonstrated [17,21,22] that there is actually a high level of iron in clusters and that this is not due to spatial convolutions occurring during ECAP analyses.

The presence of iron in clusters has also been considered in terms of 'ballistic dissolution of clusters'.

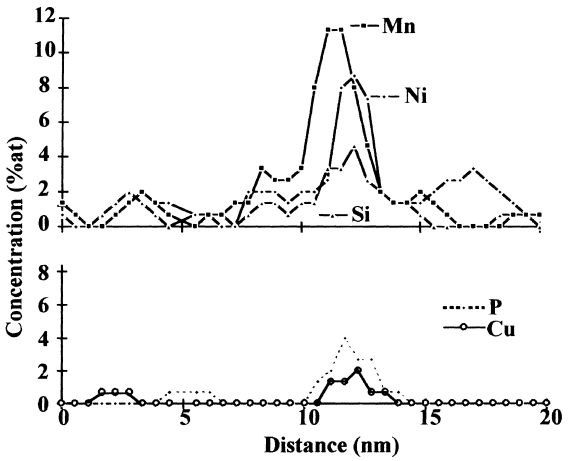

Fig. 3. Solute concentration profiles (Si, Ni, Mn, Cu and P) through a solute cluster, as determined by ECAP analysis (Chooz A steel, 12×10^{19} n cm^{-2}).

Indeed, it is known that, if irradiation can induce segregation it can also dissolve particle via atomic collision. However, the low flux involved in these irradiations cannot explain the presence of iron. The probability that two cascades collide with the same cluster in less time for the solutes to diffuse back into the cluster, is about zero [17].

Table 4
Mean composition and average and maximum solute enrichment ratio (ratio of the concentration measured in the cluster over the concentration in the matrix (given in Table 7)) of clusters encountered in the ferrite matrix of the irradiated specimen (Chooz A, 12×10^{23} n m^{-2}) as measured by AP

Elements	Si	Ni	Mn	Cu	Fe
X (at.%)	4.8 ± 0.7	3.6 ± 0.6	3.8 ± 0.7	0.9 ± 0.3	Balance
Average enrich. ratio	$\leqslant 8$	$\leqslant 6$	$\leqslant 4$	$\leqslant 22$	–
Max enrich. ratio	$\leqslant 12$	$\leqslant 12$	$\leqslant 6$	$\leqslant 60$	–

Surprisingly, [1] copper does not seem to be the major agent although in terms of enrichment ratio (see Table 4) it comes first (4–5 times higher than Mn or Ni).

Features of the same nature (composition, size) were also observed (with TAP) in two other french neutron irradiated pressure vessel steels (Dampierre 2 and Dampierre 4). These steels are fully bainitic with compositions close to that of the Chooz A steel [23].

3.2.2. Evolution of clusters with the neutron fluence

Similar investigations were applied to five other specimens of the same steel irradiated at various fluences (from 0.5 to 16×10^{19} n cm^{-2}). Except for the lowest fluence, all of the irradiated specimens exhibit the same kind of clusters as previously described. Moreover, the size and the composition of these clusters remain constant. Conversely, their number density increases with the neutron fluence (Table 5).

It must be noted that this constant size and this evolution of the number density as a function of the fluence are corroborated by SANS experiments carried out on the same specimens [22].

3.2.3. Discussion of the formation and the nature of these clusters

These clusters which are obviously (non-equilibrium features), do not evolve with time (in size and composition) during the neutron irradiation. One would have expected a growth and/or a coalescence regime instead of a 'stationary nucleation'. The basic process must be complex: formation of clusters with increasing fluence, and simultaneously stabilisation of previously existing clusters in a certainly non-equilibrium form despite the important incoming energy supplied by the incident neutrons.

Table 5
Mean size and number density of solute clusters for various fluences as measured by AP (Chooz A steel)

Fluence ($E > 1$ MeV, 10^{23} n m^{-2})	Size (nm)	Number density (10^{23} m^{-3})
2.5	3	3
6.6	3	5
12	4	9
16	3	11

Moreover, the composition of these clusters raises some questions. Although the solubility limit of copper is not precisely known at 300°C (most likely ~0.007 at.% [17,23]), it is well recognized that the ferrite matrix is supersaturated with copper. Conversely, solutes such as silicon, nickel as well as manganese (Si > 8 at.%, Mn ~ 3 at.%, Ni ~ 5 at.% at 300°C) are initially not in supersaturation, and their presence in clusters is therefore surprising.

Taking these remarks into consideration it appears that, although its content in clusters is not intrinsically high, copper plays an important role in the studied process. In order to assess this hypothesis, the present results have been compared to some others extracted from literature. Only considered in this comparison are those studies performed on ferritic steels, as well as on Fe–Cu alloys for which the copper content is low enough ($\leqslant 0.2$ at.%) so as to be regarded as similar to that encountered in French pressure vessel steels. These various experimental results were obtained from AP and SANS measurements [17,24,27]. Ten steel specimens and two Fe–Cu alloys have been considered. Fig. 4 displays these results in terms of precipitated atomic fraction of copper as a function of the neutron fluence.

The trend is clear: the percentage of the nominal copper content detected in clusters is increasing with the neutron fluence; a $\Phi^{0.23}$ function is a good approximation of this trend (where Φ is the fluence, 10^{23} n m^{-2}). Thus, the majority of the copper atoms are gathered into clusters, with rapid kinetics at the beginning of the process, followed by a slow variation reaching a 'precipitated' copper atomic fraction of about 60 at.% (±20

[1] Previous microstructural work undertaken on this problem [24,25 (non-exhaustive list)] (using principally SANS technique) was done using high copper steels, such as US weld for instance (3–4 times much more copper than here) or Fe–Cu model alloy specimens. From this approach came out a paradigm identifying copper precipitation as the factor responsible for the observed embrittlement. Our experimental observations tend to slightly modify this paradigm, at least for steels with a low copper content (<0.1 at.%). It must be noticed that the similar formation of solute clusters under neutron irradiation has been reported in a variety of US RPV welds and steels [26–28]. These latter studies were also performed using the AP.

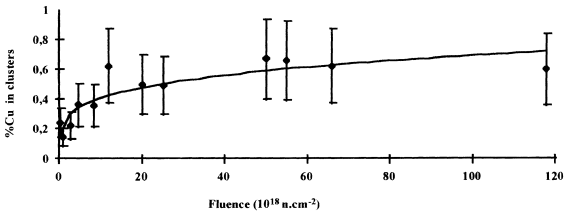

Fig. 4. Evolution of the atomic fraction of copper observed in the irradiation induced particles with the neutron fluence for 10 steel specimens and two Fe–Cu alloys.

at.%) for high fluences (1×10^{24} n m^{-2}). As an example, the copper content remaining in the ferrite solid solution is, for the Chooz A steel, close to 0.03 at.% for a fluence of 5×10^{19} n cm^{-2}. That is to say 57% of copper atoms are localised into clusters.

Taking into account the fact that the solute concentration in clusters is more or less constant during the irradiation process, it comes out that the enhancement in atomic fraction of precipitated copper is due to the increase in the number density of formed clusters.

The microstructural changes in a material under energetic neutron irradiation are caused by atoms expulsed from their lattice sites (Primary Knock on Atoms (PKA), then secondary, and so on...). Along the path of the PKA freely migrating point defects are created. A cascade of displacements takes place at the end of the motion of the PKA. When the energy is between 1 and 5 keV, its mean free path becomes comparable with the interatomic distances. A considerable number of atoms is therefore displaced inside a volume of about 10 nm in diameter [29]. The results obtained from numerical simulations greatly contribute to the understanding of the morphology and time dependent evolution of the displacement cascades. Having in mind this schematic view of the neutron irradiation damage, several tentative scenarios can be proposed to explain the formation and the development of clusters:

- The number density of clusters is correlated with the number of displacement cascades. This suggests an important role of cascades in the formation of clusters. The mechanism could be a direct agglomeration of solutes after a few seconds of the atom mixing and the collapse of the cascade. This collapse of cascade is indeed caused by complex mechanisms of recombination of defects which could lead in turn to the migration of solutes towards the cascade centre. This could explain the segregation of supersaturated copper atoms into clusters but not so easily the concomitant segregation of other species like silicon, nickel and manganese [17,22].
- Qualitatively, segregation of these species may be due to vacancy flux towards the core of the cascade which act as a sink (small void or vacancies trapped with copper atoms). Then, an induced atom flux (inverse Kirkendall effect) could lead to the observed local solute (Cu, Si, Ni, Mn, Ni) enrichments. As the Si, Ni, Mn contents are under the solubility limits in α-ferrite, this local enrichment is in principle not stable. This leads to outward fluxes giving rise to an opposite effect as compared to the inverse Kirkendall effect: the dissolution of clusters. It is thought that a dynamic equilibrium may be reached by balancing both inward and outward fluxes. This mechanism implies enhanced diffusion (for copper which is supersaturated), induced segregation and also dissolution (for under-saturated solutes) [30].
- Another proposal [31] could be the formation of dislocation loops created by interstitials. Contrary to vacancies, an interstitial flux always induces atom fluxes in the same direction. Thus, components which are transported preferentially by interstitial are always enriched at the sink. This mechanism also involves competition between growth and dissolution processes.

These hypotheses lead to the possible existence of irradiation-induced defects like small vacancy clusters, solute-defect complexes, interstitial dislocation loops, etc. These tiny microstructural events are difficult to be observed by AP. For the Chooz A irradiated steel, they were not directly observed by TEM [32], may be because of the weak contrast. High resolution experiments were performed [32] on irradiated materials. The presence of defects (3 nm in diameter) was revealed by local enhancements of contrast. Distorsions of atomic planes were observed in such zones with enhanced contrast. PA proved the existence of such small vacancy–copper complexes in the case of a Fe–0.1 at.% Cu alloy irradiated with electrons [33].

4. Copper segregation in irradiated Fe–Cu model alloys

4.1. Introduction

The latter discussion has pointed out the role of copper, even in this low copper ferritic steel. In order to decrease the number of parameters that could operate, two main simplifications were performed:

- Focusing on the role of copper, Fe–Cu alloys with various levels of supersaturation have been studied.
- In addition to neutron irradiation, which is a rather heavy mean of irradiation (need of a reactor plus activity and waste problems) and complex to understand (competition between several processes)), electron and ion irradiations were carried out. Electron irradiation is known for promoting the formation of a large amount of Frenkel pairs. The transferred energy from incident particles to target atoms is not high enough to produce displacement cascades. Conversely, ion irradiation allows the

formation of displacement cascades, with the advantage, as compared to neutron irradiation, that the energy spectrum of incident projectiles is well defined. Thus, the physics of interactions are 'better' understood. In addition, with energies here involved, samples are not activated.

4.2. Materials

A low supersaturated Fe–Cu model alloy, the copper content of which is close to that of french pressure vessel steels (~0.1 at.% Cu), as well as two highly supersaturated Fe–Cu alloys (~1.4 at.% Cu), were manufactured by CECM (Vitry, France) from a high purity ingot (C < 15 ppm, N < 10 ppm, Si < 25 ppm). The samples were cold-rolled and austenitized at 1000°C for 30 min. The alloys were then heat treated in vacuum for 1 h at 850°C and quenched to produce a reference random solid solution. EDX measurements revealed copper contents of 0.09 ± 0.03 at.% (1), 1.38 ± 0.10 at.% (2) and 1.34 ± 0.04 (3) respectively.

Electron irradiations were carried out with a Van de Graaff accelerator (1) at CEN–Grenoble–France with 3 MeV electrons, or (3) at CEA/DTA/CEREM/DTM-Ecole Polytechnique–Palaiseau–France with 2.5 MeV electrons ($\sim 5.4 \pm 10^{-5}$ NRT dpa). The irradiation temperatures were kept constant to 290°C which is the service temperature of RPV steels.

Neutron irradiations were also performed in the Osiris pool test reactor (CEN–Saclay–France) at a target temperature of 290°C (samples (1) and (2)) with a flux of 2.8×10^{13} n cm^{-2} s^{-1} to reach a fluence of 5.5×10^{19} n cm^{-2} ($E > 1$ MeV). This corresponds to about 75 NRT mdpa.

A preliminary ion irradiation was undertaken on the Fe–0.1 at.% Cu alloy using the ion accelerator of the Hahn-Meitner-Institut (Berlin) [34]. The irradiation was directly performed on AP specimens (sharp needles), perpendicular to the needle axis with 300 keV Fe^+ ions at room temperature. The irradiation duration (10 s) was calculated to reach a fluence of 10^{-2} NRT dpa (order of magnitude of NRT dpa encountered in RPV steels).

4.3. Experimental results

4.3.1. Highly supersaturated Fe–Cu alloys (~1.4 at.% Cu)

Fig. 5(a) and (b) exhibits two reconstructed volumes of TAP analyses performed in these electron (a) and neutron (b) irradiated alloys. For the sake of simplicity, only copper atoms are represented. Associated copper concentration profiles can be drawn through particles as displayed by Fig. 5(c) (electron irradiation) and (d) (neutron irradiation).

For both types of irradiation carried out at 300°C, copper-rich particles are formed. Sizes, as well as the number density of particles are of the same order of magnitude. In the electron-irradiated specimen, the mean particle diameter is ~2 nm and the number density is $\sim 1 \times 10^{24}$ m^{-3}. In the neutron-irradiated specimen the same parameters are ~2–4 nm and $\sim 2 \times 10^{24}$ m^{-3}, respectively. These values were confirmed by SANS experiments [22,36].

Beyond these similarities, differences exist. As shown by Fig. 5(c), it appears that particles formed during electron irradiation are quasi-copper-pure, i.e., they are in the expected equilibrium form as it might happen after a heat treatment. Electron irradiation therefore enhances the atomic mobility of copper atoms at 300°C and promotes accelerated precipitation. This enhanced diffusion mobility of atoms induced by the increase in point defect concentration under electron irradiation has been discussed by Smetniansky-de-Grande and Barbu [37] on the basis of studies carried out with different electron fluences. SANS, microhardness and electrical resistivity experiments allowed one to determine a copper diffusion coefficient, $D_{\text{electron irrad}} = 1.2 \times 10^{-18}$ cm^2 s^{-1}, under electron irradiation (290°C, 4×10^{13} e$^-$ cm^{-2} s^{-1}) which could be compared to the 'extrapolated' value of the thermal diffusion coefficient at 300°C ($D_{\text{thermal}} = 2.2 \times 10^{-24}$ cm^2 s^{-1}).

Conversely, Fig. 5(d) exhibits particles, the copper content of which is not 100%. There is a large variability of compositions from 45 to 95 at.% Cu with a mean copper concentration of 72 at.%. The neutron irradiated alloy does not seem to reach an equilibrium state.

The difference of copper content between one particle and another could be attributed to a difference in their 'date of birth' (or nucleation); the older being the richer. This appears to be a specific effect of neutron irradiation. Displacement cascades could act as preferential nucleation sites as already mentioned above (steels). Nevertheless, there is also a contribution of the diffusion mechanism which accounts for the copper enrichment of particles with time or fluence. This latter contribution should then be attributed to a large freely migrating point defects population.

A great difference also exists between the matrix composition of electron and neutron irradiated specimens. After electron irradiation (5.4×10^{-5} NRT dpa), the copper remaining in solid solution is 0.7 ± 0.1 at.%, while after neutron irradiation (7.5×10^{-2} NRT dpa), it is as low as 0.08 ± 0.02 at.%. Such a difference may be due to the addition of the two separate previously depicted processes. Indeed, neutron irradiation creates a large number of nucleation sites (core of cascades) and also enhances the copper diffusion. This last indication is in good agreement with the calculated NRT dpa for each cases. However, it is recognized that, for a

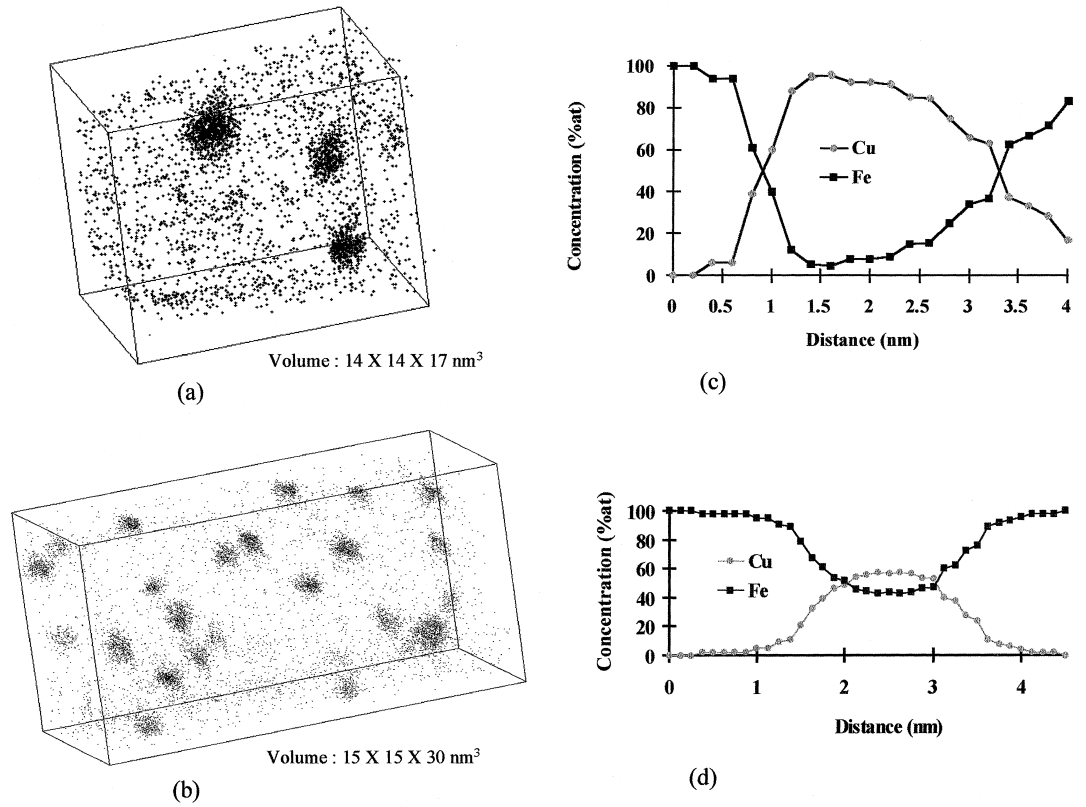

Fig. 5. Cu-rich irradiation induced clusters: (a) and (c) For electron irradiation; (b) and (d) for neutron irradiation; (left) 3D TAP reconstruction; only copper atoms are represented, one dot is one atom (only 50% of atoms are collected by the detector); (right) Concentration profiles for Fe and Cu through one particle.

calculated NRT dpa value, neutron irradiation creates much fewer freely migrating point defects than electron irradiation ($\sim 10^2$ times less because of recombination processes). One should then compare 5.4×10^{-5} NRT dpa (for electron) to 7.5×10^{-4} 'corrected' dpa (for neutron). This shows that the dpa number for neutron is about ten times higher than for electron. We should therefore have more well-developed and larger particles with sharp interfaces. This is not the case. This shows again a specific effect of the displacement cascades. Some similar experimental results have been reported by [35,36].

4.3.2. Low supersaturated Fe–Cu alloys (~0.1 at.% Cu)

This model alloy was chosen because its copper content (0.09 at.%) was close to that of the Chooz A steel (0.08 at.%). These values are, nevertheless, higher than the supposed solubility limit of copper in α-iron at 300°C (~0.007 at.%). After irradiation, the experimental observations, as shown by TAP results, are clear:

- electron irradiation ($E \sim 3$ MeV, 290°C, 2×10^{19} e^- cm^{-2}, 1.2×10^{-3} NRT dpa) does not modify the solute partition. Copper atoms remain randomly distributed in the α-iron solid solution. Conversely
- after neutron irradiation ($E > 1$ MeV, 290°C, 5.5×10^{19} n cm^{-2}, 7.5×10^{-2} NRT dpa), some small copper-enriched clusters are formed (Fig. 6).

These copper-enriched clusters have diameters in the range 2–3 nm and a number density of about 1×10^{23} m^{-3}. They exhibit a large variability of compositions; the mean value being $\sim 35 \pm 5$ at.% Cu. The matrix solid solution is copper depleted down to 0.03 ± 0.01 at.% Cu. These results have been confirmed by SANS experiments [22]. Similar results have been previously correlated to SANS [38] and to ECAP [39] experiments.

Here again, and perhaps more convincingly, the specific effect of displacement cascades which are signatures of neutron irradiation, is shown. With a corrected number of dpa (7.5×10^{-4} corrected dpa) lower than the one calculated for electron irradiation (1.2×10^{-3} NRT dpa), segregation of copper is observed.

4.3.3. Ion irradiation

The same Fe–Cu (~0.1 at.% Cu) alloy was also irradiated by 300 keV Fe^+ ions at room temperature

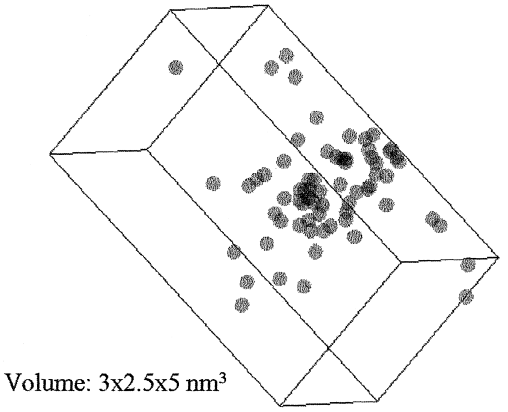

Fig. 6. 3D TAP reconstruction of a small Cu-rich cluster formed after neutron irradiation ($E > 1$ MeV, 290°C, 5.5×10^{19} n cm^{-2}, 7.5×10^{-2} NRT dpa). Only Cu-atoms (50%) are represented, one sphere is one atom.

up to a fluence of $\sim 10^{-2}$ NRT dpa. After irradiation, the specimen was analysed using the TAP technique and the results compared to those of the unirradiated material. Because of the extremely weak effect of the irradiation, only statistical treatments of AP data evidence an evolution of the solid solution [34] (Fig. 7).

The number of copper atoms in the biggest cluster could be estimated (close to 20). The number density of clusters was found close to 1×10^{23} m^{-3}. The comparison with neutron irradiation is of interest. Indeed, the achieved fluence is 7–8 times lower for ion irradiation. Nevertheless microstructural evolution within the solid solution occurs. This could be the very initial stage of the process, that is to say the nucleation of copper-enriched clusters. The amplitude of clustering is still too weak for the copper level in the solid solution to decrease significantly. Within experimental uncertainties, the copper level in the solid solution remains close to the nominal composition.

4.4. Conclusion

Both low and high supersaturated materials decompose under neutron irradiation. The copper contents are most likely dependant on the nominal concentration and also on the fluence. The alloys do not reach a steady state even after a long fluence irradiation. This appears to be a specific effect of displacement cascades (acting as nucleation sites?) as well as an increase of the atomic mobility promoted by the creation of freely migrating defects. For long-term treatments, the α-iron solid solution is copper depleted down to values close to 0.03 at.%. This value remains higher than the estimated copper solubility limit in α-iron at 300°C. It is, however, close to that encountered in neutron irradiated steels.

Electron irradiation leads to a different scheme. It acts only through the increase of the number of freely migrating defects; it promotes accelerated precipitation. Nevertheless, it does not seem to be able to initiate copper precipitation under a certain supersaturation threshold (between 0.1 and 0.2 at.% Cu).

This demonstrates the decisive role of displacement cascades formed by neutron (ion) irradiation. These are thought to be involved in the cluster nucleation process through atomic mixing and cascade collapse, or more indirectly through the remaining defect aggregates formed after cascade collapse.

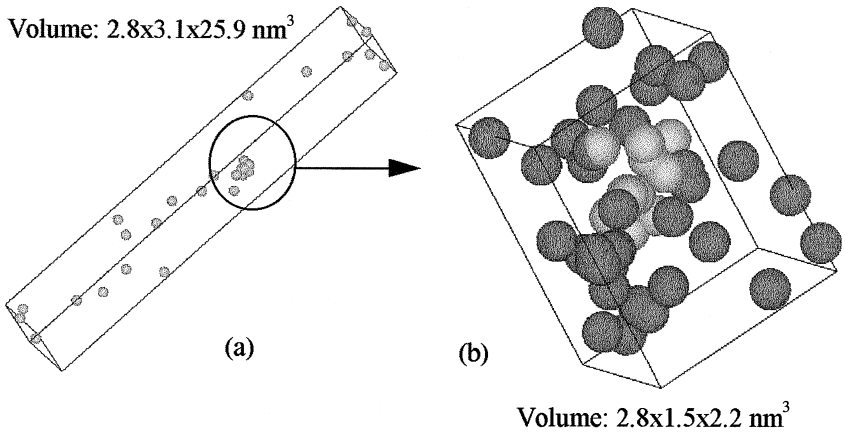

Fig. 7. (a) 3D TAP reconstruction of the Fe–0.1 at.% Cu model alloy after Fe-ion irradiation (300 keV, 20°C, 0.01 NRT dpa). Only Cu-atoms (50%) are presented. (b) Enlargement of the small cluster exhibited in (a). Cu-atoms are light grey and Fe-atoms are dark grey.

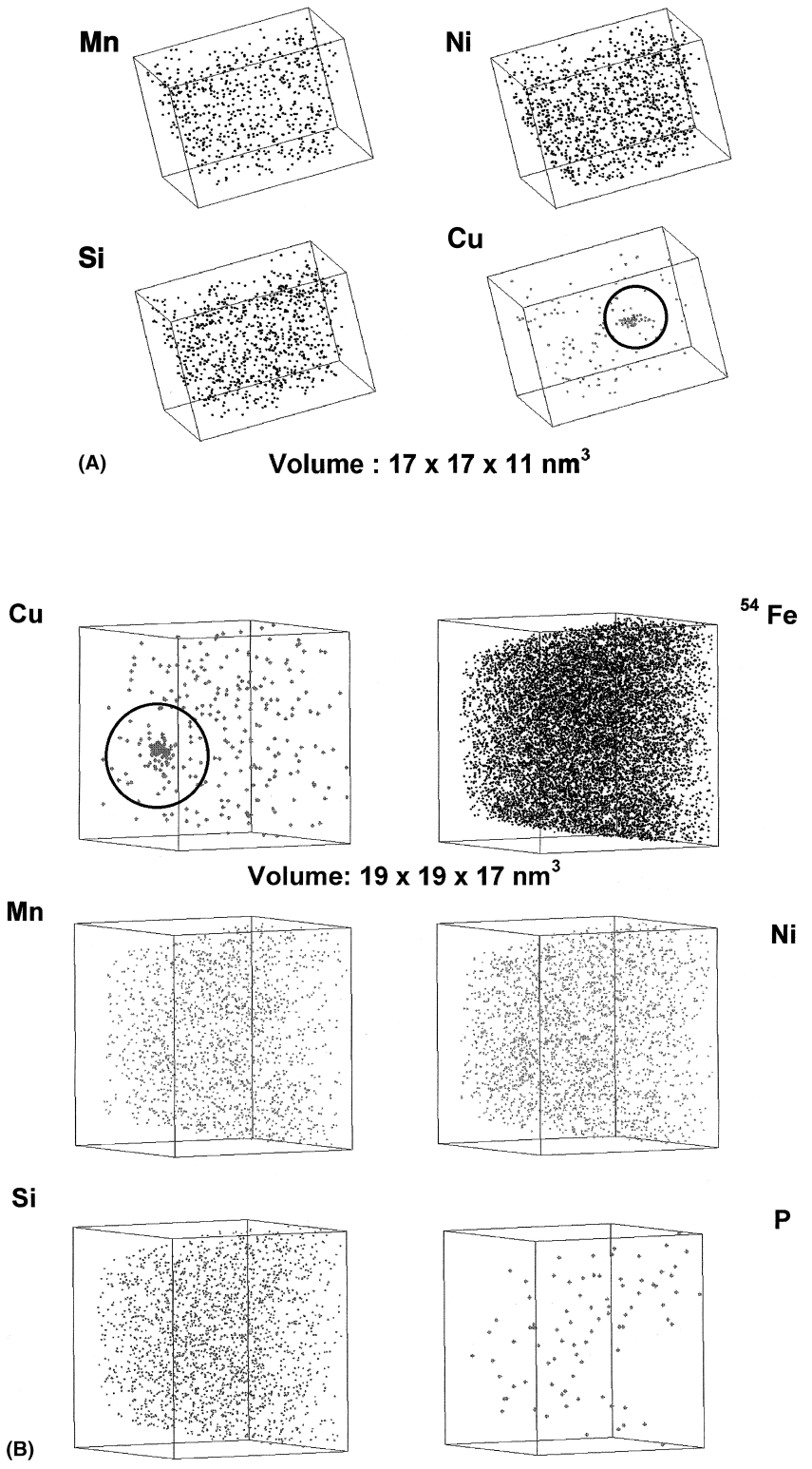

Fig. 8. (A) 3D TAP reconstruction of the irradiated Chooz A material annealed at 450°C for 2 h. Copper clusters are observed with no associated Ni, Mn, and Si. (B) 3D TAP reconstruction of the irradiated Chooz A material annealed at 450°C for 100 h. Copper clusters observed in the 2 h annealed materials are growing as pure copper particles.

5. Recovery of mechanical properties of RPV steels: Annealing treatments

Thermal annealing treatments have been identified as a suitable means to recover the mechanical properties (Charpy upper shelf energy and ductile-to-brittle transition temperature) of embrittled RPV steels. A previous study [3] showed that a reasonable compromise between the highest degree of recovery and an acceptable annealing time at a technically achievable temperature could be found (450°C for a few hundred hours). Such treatments were applied to previously irradiated (13 years) specimens of the Chooz A steel.

Microhardness measurements were undertaken to follow the mechanical recovery. It was shown that after ~20 h of annealing, the reference level (hardness measurement of the unirradiated material) is reached [23].

TAP experiments were carried out on specimens annealed at 450°C during 2 and 100 h. These specimens were previously irradiated (12×10^{19} n cm^{-2}, $\sim 16.5 \times 10^{-2}$ NRT dpa) and exhibited a high density (9×10^{17} cm^{-3}) of solute clusters (Cu ~ 0.9, Si ~ 4.8, Mn ~ 3.8, Ni ~ 3.6 at.% with additions of P, Cr, ...) dispersed in the ferritic solid solution (remaining Cu content 0.04 at.%).

The first experimental observation which arises from this study is the dissolution of the solute clusters, even after only 2 h of annealing treatment at 450°C (Fig. 8(A)).

The second experimental evidence is the formation of a low number density ($< 0.1 \times 10^{23}$ m^{-3} after 100 h of annealing) of Cu-rich precipitates, the size and copper content of which increase with the annealing treatment duration (Fig. 8(B)).

The third point is the stability of the copper content of the solid solution (~0.04 at.%).

These atom probe results are displayed in Tables 6 and 7.

In addition, it must be noted that the interface between the analysed copper particles (100 h at 450°C) and the solid solution is enriched with nickel and manganese atoms. This was also observed in a weld material under similar conditions [40].

Attention must be paid to the evolution of the Cu content of the ferrite solid solution. After irradiation, the Cu-concentration is 0.04 at.% and remains at the same level after the annealing treatment while solute (Cu, Ni, Mn, Si, ...) clusters dissolve and Cu-rich precipitates are formed. Moreover, this value (0.04 at.%) is known to be very close to the solubility limit of copper in α-iron at 450°C [17,23] which is 0.05 at.%. The first

Table 6
Characterisation of solute clusters encountered in the Chooz A steel after (1) neutron irradiation (12×10^{23} n m^{-2}), (2) neutron irradiation and annealing treatment 2 h at 450°C and (3) neutron irradiation and annealing treatment 100 h at 450°C; AP results (TAP)

Specimen	Cluster mean diameter (nm)	Cluster composition (at.%)	Cluster number density (10^{23} m^{-3})
(1)	3–4	Cu ~ 0.9; Ni ~ 3.8; Mn ~ 3.8; Si ~ 4.8	9
(2)	1–2	Cu ~ 30; Fe balance	Not determined
(3)	3–4	Cu > 60; Fe balance	~0.1

Table 7
Chemical composition of the ferrite solid solution (clusters extracted) of the Chooz A steel for the four stages: (0) unirradiated specimen, (1) neutron irradiated (12×10^{23} n m^{-2}), (2) neutron irradiated and annealed 2 h at 450°C and (3) neutron irradiated and annealed 100 h at 450°C; these are AP results

Specimen	C	P	Si	Cr	Mo	Mn	Ni	Cu	Fe
(0)									
at.%	0.05	0.02	0.80	0.15	0.26	1.32	0.68	0.08	Balance
2σ	0.02	0.01	0.10	0.04	0.06	0.13	0.10	0.03	–
(1)									
at.%	0.05	0.02	0.62	0.13	0.22	1.00	0.66	0.04	Balance
2σ	0.01	0.01	0.05	0.02	0.03	0.05	0.05	0.01	–
(2)									
at.%	0.02	0.02	0.59	0.10	0.12	1.10	0.64	0.05	Balance
2σ	0.01	0.01	0.06	0.03	0.03	0.08	0.05	0.01	–
(3)									
at.%	0.01	0.01	0.57	0.16	0.17	1.20	0.75	0.04	Balance
2σ	0.01	0.01	0.05	0.03	0.03	0.07	0.05	0.01	–

possible explanation is that the formation of Cu-rich precipitates is probably directly related to the dissolution of the irradiation-induced solute clusters, from which they get their copper atoms. These solute clusters act as preferential nucleation sites for copper precipitation. The driving force is low and therefore, homogeneous nucleation is difficult to attain (the critical size is equivalent to 80 Cu-atoms considering a regular solid solution model [17]). As a result, one could imagine that only clusters with the highest amount of copper could really act as efficient nuclei for the formation of equilibrium copper precipitates. The number of such clusters, acting as preferential sites, may be much smaller than the total number of neutron-induced clusters. All the others will dissolve to increase the size of the largest. A growth and coarsening regime is then taking place. The presence of some enhancements of Ni, Mn, Si concentrations in the surroundings of the Cu-rich particles after 100 h of annealing may be due to the rejection of solutes from the core of the particles toward the periphery during the growth regime [41] or to a strong copper and/or vacancy solute trapping.

These experimental observations show that annealing treatments cause the dissolution of neutron-induced clusters. They also indicate that the low number density of copper precipitates formed in the ferrite matrix after annealing has little influence on the mechanical properties of the recovered material. Therefore, if annealing treatment leads to a low number density of nearly pure copper particles and a low matrix copper content, further neutron irradiation of these irradiated and annealed materials should not produce a large transition temperature shift. This will show the importance of point defects, grain boundary segregation and perhaps local-induced segregations but without copper!

6. Conclusion

Although not complete yet, knowledge about solute segregation induced by neutron irradiation in RPV steels have considerably increased in the past. The copper content is a determinant parameter even in the case of low copper steels (<0.1 at.%). Solute-defect clusters (Cu, Ni, Mn, Si, P, ...) are formed during irradiation with a number density which increases with neutron fluence. According to some other studies, the mean Cu content of these solute clusters appears to be closely related to the Cu-nominal concentration of the RPV steel.

Displacement cascades formed during neutron irradiation may be directly involved in the clustering process; the damaged areas could act as nucleation sites. The actual process of cluster formation is not fully understood yet. This could happen directly by atom mixing inside the displacement cascades or by an induced segregation process moving solute atoms towards the core of collapsed cascades acting as sinks.

The solute clusters are probably associated with point defects, which could explain their rather high hardening efficiency. Of course, other irradiation-induced defects are also formed such as point defects and grain boundary segregation, ... which also participate to the increase of embrittlement.

Rather short annealing treatments (20 h at 450°C for the Chooz A steel), are sufficient to fully recover the mechanical properties (in terms of hardness decrease). The associated microstructural evolution consists in the dissolution of a high density of solute-enriched clusters and the precipitation of a low density of Cu-rich particles.

Further neutron irradiation of these annealed materials could be thought to be less prone to embrittlement. Further investigations are planed to elucidate these issues.

Acknowledgements

The authors wish to thank EDF SCMI (Avoine, France) and EDF 'Les Renardières' (Moret sur Loing, France) for providing samples and Drs A. Barbu, G. Martin, M. Akamatsu and S. Miloudi for fruitful discussions. This research work was financially supported by EDF (contract EDF/CNRS no. 508914) which we wish to thank.

References

[1] A.D. Amayev, A.M. Kryukov, M.A. Sokolov, in: L.E. Steele (Ed.), Radiation Embrittlement of Nuclear Reactor Pressure Vessel steels, An International Review, Fourth Volume, ASTM STP 1170, ASTM, Philadelphia, PA, 1993, p. 369.
[2] A.M. Kryukov, M.A. Sokolov, in: W.R. Corwin, F.M. Haggag, W.L. Server (Eds.), Small Specimen Test Techniques Applied to Nuclear Reactor Vessel Thermal Annealing and Plant Life Extension, ASTM STP 1204, ASTM, Philadelphia, PA, 1993, p. 417.
[3] S.K. Iskander, M.A. Sokolov, R.K. Nanstad, in: D.S. Gelles, R.K. Nanstad, A.S. Kumar, E.A. Little (Eds.), Effects of Radiation on Materials, 17th International Symposium, ASTM STP 1270, ASTM, Philadelphia, PA, 1994, p. 277.
[4] J.M. Sarrau, F. Danoix, B. Deconihout, M. Bouet, A. Menand, D. Blavette, Appl. Surf. Sci. 76/77 (1994) 363.
[5] M.K. Miller, P. Pareige, M.G. Burke, Mater. Charact. (44) (2000) 235.
[6] U. Potapovs, J.R. Hawthorn, Nucl. Appl. 6 (1) (1969) 27.
[7] M.K. Miller, M.G. Burke, J. Phys. C 6 (1987) 429.
[8] E.W. Müller, J.A. Panitz, S.B. McLane, Rev. Phys. Instrum. 39 (1968) 83.

[9] M.K. Miller, A. Cerezo, M.G. Hetherington, G.D.W. Smith, Atom Probe Field Ion Microscopy, Clarendon, Oxford, 1996.
[10] D. Blavette, B. Deconihout, A. Bostel, J.M. Sarrau, M. Bouet, A. Menand, Rev. Sci. Instrum. 64 (10) (1993) 2911.
[11] F. Hedin, M. Bauge, B. Guilleret, B. Barthelet, in: Proceedings of the International Nuclear Power Plant Aging Symposium, Bethesda, Maryland, USA, 1988.
[12] C. Brillaud, Rapport EDF-SCMI D.5004/BRD/R 88.07, 1988.
[13] M.J. Norgett, M.T. Robinson, I.M. Torrens, Nucl. Eng. Des. 33 (1975) 50.
[14] P. Pareige, J.C. Van Duysen, P. Auger, Appl. Surf. Sci. 67 (1993) 342.
[15] P. Pareige, M.K. Miller, Appl. Surf. Sci. 67 (1996) 370.
[16] P. Auger, P. Pareige, M. Akamatsu, J. Van Duysen, J. Nucl. Mater. 211 (1994) 194.
[17] P. Pareige, doctoral thesis, Rouen University, October 1994.
[18] M.J. De Van, A.L. Lowe Jr., S. Wade, in: A.S. Kumar, D.S. Gelles, R.K. Nanstad, E.A. Little (Eds.), Effects of Radiation on Materials, 16th International Symposium, ASTM STP 1175, ASTM, Philadelphia, PA, 1993.
[19] P. Pareige, K.F. Russell, R.E. Stoller, M.K. Miller, J. Nucl. Mater. 250 (1997) 176.
[20] B. Sundman, B. Jansson, J-O. Anderson, CALPHAD: Comput. Coupling Phase Diagrams Thermochem. 9 (1985) 153.
[21] P. Auger, P. Pareige, M. Akamatsu, D. Blavette, J. Nucl. Mater. 225 (1995) 225.
[22] P. Pareige, P. Auger, S. Miloudi, J.C. Van Duysen, M. Akamatsu, Ann. Phys. C2 22 (3) (1997) 117.
[23] S. Miloudi, doctoral thesis, Université de Paris Sud (Orsay), December 1997.
[24] C.A. English, W.J. Phythian, J.T. Buswell, J.R. Hawthorn, P.H.N. Ray, in: R.E. Stoller, A.S. Kumar, D.S. Gelles (Eds.), Effects of Radiation on Materials, 15th International Symposium, ASTM STP 1125, ASTM, Philadelphia, PA, 1992, p. 93.
[25] F. Frisius, R. Kampmann, R. Wagner, P.A. Beaven, in: Proceedings of the International Symposium on Environmental Degradation of Materials in Nuclear Power Systems – Water Reactors, Monterey, 1985.
[26] M.K. Miller, D.T. Hoelzer, F. Ebrahimi, J.R. Hawthorn, M.G. Burke, J. Phys. C6, sup. no. 11, tome 48 (1987) 423.
[27] M.G. Burke, M.K. Miller, J. Phys. C6, sup. no. 11, tome 49 (1988) 283.
[28] M.G. Burke,S.S. Brenner, J. Phys. C2, sup. no. 3, tome 47 (1986) 239.
[29] A. Dunlop, F. Rullier-Albenque, C. Jaouen, C. Templier, J. Davenas (Eds.), Materials under Irradiation, TransTech, Gedermannsdorf.
[30] P. Pareige, private communication.
[31] A. Hardouin Duparc, A. Barbu, Mater. Res. Soc. Symp. Proc. 439 (1997) 509.
[32] J.C. Van Duysen, J. Bourgoin, P. Moser, C. Janot, Radiation embrittlement of nuclear reactor pressure vessel steels, AIEA, Balatonfured, Hungary, 1990.
[33] M. Akamatsu, J. Van Duysen, P. Pareige, P. Auger, J. Nucl. Mater. 225 (1995) 192.
[34] P. Pareige, S. Welzel, P. Auger, J. Phys. C5 6 (1995) 229.
[35] M.H. Mathon, doctoral thesis, Paris XI Orsay University, March 1995.
[36] J.T. Buswell, C.A. English, M.G. Hetherington, W.J. Phythian, G.D.W. Smith, G.M. Worall, ASTM STP 1046 (1990) 127.
[37] N. Smetniansky-de-Grande, A. Barbu, Radiat. Eff. Point Def. in Solids (1994).
[38] P.A. Beaven, F. Frisius, R. Kampman, in: International Symposium on Environmental Degradation of Materials in Nuclear Power systems and Water Reactors, ANS, 1986, p. 400.
[39] M.K. Miller, K.F. Russell, A. Jostsons, R.G. Blake, Appl. Surf. Sci 87&88 (1995) 216.
[40] P. Pareige, R.E. Stoller, K.F. Russell, M.K. Miller, J. Nucl. Mater. 249 (1997) 65.
[41] P. Pareige, K.F. Russell, M.K. Miller, Appl. Surf. Sci. 94&95 (1996) 362.